Front. Mater. Sci. 2022, 16(3): 220614
https://doi.org/10.1007/s11706-022-0614-8

RESEARCH ARTICLE

Electroactive chitosan-aniline pentamer hydrogel for peripheral nerve regeneration

Deqiang MIAO, Ya LI, Zhongbing HUANG (✉), Yulin WANG, Min DENG, and Xiaohui LI

College of Biomedical Engineering, Sichuan University, Chengdu 610065, China

ABSTRACT: Electroactive hydrogels could guide the regeneration of nerves and promote their functional recovery. An aniline pentamer-crosslinked chitosan (CS-AP) hydrogel with better electroactivity and degradation was fabricated by the carbodiimide method, and then injected into the repair site of sciatic nerve damage, with its gelation time, tensile strength, and conductivity reaching 35 min, 5.02−6.69 MPa, and from 2.97×10^{-4} to 3.25×10^{-4} S·cm^{-1}, respectively, due to the cross-linkage and well-distribution of AP. There was better cytocompativility of CS-AP hydrogel on nerve cells. The results of the *in vivo* repair indicated that CS-AP10 hydrogel induced the capillaries formation and the repair of sciatic nerve defect, and re-innervated gastrocnemius muscle in the CS-AP10 group were obviously better than other experimental groups, due to the electroactivity of CS-AP and its degradation into fragments. These results indicated the potential application of CS-AP hydrogel in the regeneration and function recovery of peripheral nerve injury.

KEYWORDS: peripheral nerve regeneration; chitosan; aniline pentamer; electroactive hydrogel; capillary formation

Contents

Received April 10, 2022; accepted June 2, 2022

E-mail: zbhuang@scu.edu.cn

1 Introduction

Peripheral nerve injury as a global problem seriously impacted patients' life quality [1]. Severe injuries needed

to be surgically treated and the autograft was the gold standard for peripheral nerve repair [2]. However, autologous nerve grafting could lead to the worse function of reinnervation, secondary damage, and the potential neuroma formation at the donor site [3]. Thus, tissue engineering strategy for the peripheral nerve injury focused on the development of nerve scaffold conduit of degradable materials [4–5].

Conductive polymers (CPs) were attractive scaffold materials in tissue engineering, because CPs not only had biocompatibility and electroactivity, but also easy preparation and simple modification [6]. It was reported that nerve neurites easily adhered on the hydrophilic modified CPs electrically to stimulate with them for the promotion of the axons growth [7]. Furthermore, electroactive polymers could also promote cellular activity, cell adhesion, migration and proliferation, due to their effect on the internal environment of cell growth [8–9], and some CPs were used to prepared scaffold conduits for nerve repair, although there were some challenges [10].

Polyaniline (PANI) and its composites were applied in nerve tissue engineering, due to its semi-conductivity, easy modification and good cyto-compatibility on endothelial cells and nerve cells [11]. Liu et al. achieved an assembly product of PANI and poly 3,4-ethylenedioxythiophene (PEDOT) on specified cellular elements, which could not only maintain neuronal viability but also remodel membrane properties [12]. However, the polymer chain of PANI was non-degradable and poorly soluble, which greatly limited their application in tissue engineering. Therefore, much attention was drawn to aniline oligomers, including aniline tetramer (AT) and aniline pentamer (AP) [13–14], which could be metabolized out of the body, avoiding re-operation or the long-term untoward effect *in vivo*, thus leading to their potential application in tissue engineering [15], including myocardium muscle and bone [16–17]. It was reported that a variety of factors, such as the degree of oxidation of the polymer, type of dopant, morphology of the polymer chains and chain length, could significantly influence the conductivity of PANI [18]. Guo et al. synthesized a hyperbranched copolymer based on poly ε-caprolactone (PCL) and carboxyl-capped aniline pentamer (CCAP) with the electrical conductivity from 0.2×10^{-6} to 5×10^{-6} $S \cdot cm^{-1}$, which was adequate to deliver bioelectrical signals *in vivo* [19].

Chitosan-based hydrogel scaffold could provide an environment similar to the extracellular matrix with a highly porous and interconnected structure, which allowed the encapsulation of growth factor and exchange of nutrients [20]. What's more, a large amount of $-NH_2$ groups in chitosan chains led to its unique polycationic nature and facilitated the opportunity to introduce CPs segments into its main chain [21].

Angiogenesis was also an essential component of nerve regeneration. In nerve repair progress, the increased metabolic induced local hypoxia micro-environment, and the increased neovascularization could meet the demand of nutrition supplement, because the regenerated blood vessels could accelerate the delivery of oxygen and nutrients, and the removal of the metabolic waste [22–23].

In this work, one promising hydrogel of chitosan-graft-aniline pentamer (CS-AP) with stable semi-conductivity, favorable biocompatibility and good degradability was prepared with carbodiimide method, in order to repair the nerve damage. Then their structure, composition and properties, including the conductivity, biocompatibility, and degradation, were explored with the four-probe method, cytotoxicity test and the immersion in phosphate buffered saline (PBS), respectively. Furthermore, a rat model of sciatic nerve injury was established to explore the nerve repairability of the CS-AP hydrogel *in vivo*.

2 Materials and methods

2.1 Synthesis of aniline pentamer-grafted chitosan (CS-AP)

First, carboxyl-capped aniline pentamer (CCAP) was prepared by oxidative coupling reaction, according to reference, and the preparation procedure was described in the section of ESI [24]. Secondly, chitosan was grafted with different amounts of aniline pentamer via the carbodiimide method, as shown in Fig. S1. Chitosan and the obtained aniline pentamer-grafted chitosan were called as CS, CS-AP10, CS-AP15, and CS-AP20, corresponding the rates of added AP were 0, 10, 15, and 20 wt.%, respectively, as listed in Table S1.

A typical example (CS-AP10) was as follows: AP of 0.25 g, N-hydroxysuccinimide (NHS) of 0.6188 g and 1-(3-dimethylaminopropyl)-3-ethylcarbodiimide hydrochloride (EDC·HCl) of 1.0296 g were dissolved into 40 mL of N, N-dimethylformamide (DMF), and stirred at room temperature (RT) for 24 h. Then the mixture was added dropwise into 1 wt.% of CS solution (2 g of CS was

dissolved in 200 mL of PBS), and stirred at RT for 24 h. Subsequently, the precipitation was centrifugated to remove the insoluble matter. The final product was washed five times by deionized water and obtained by lyophilization.

2.2 Characterization

FT-IR spectra of AP, and CS-AP hydrogel were recorded on Fourier transmission infrared spectroscopy (FTIR, Prestige-21 spectrometer). ^{1}H nuclear magnetic resonance (^{1}H NMR) spectra of AP and CS-AP were obtained on a 400 MHz NMR instrument (Avance II) with DMSO-d_6 as solvent at RT. Crystal structure was analyzed with X-ray diffraction (XRD, Empyrean, PANalytical). Rheology and gelation time of CS-AP10 was analyzed using AR2000EX Plate Rheometer (TA Structures Co., USA). Time sweep experiment was carried out with a frequency 1 Hz and strain of 1% at 37 °C, and a dynamic frequency sweep experiment was performed (frequency ranging from 1 to 100 rad·s^{-1} at shear amplitude of 0.1%). Cyclic voltammetry (CV) of AP and CS-AP was measured using an Electrochemical Workstation (HITACHI 660E), including a system of three-electrode, employing two platinum disks as working electrode and auxiliary electrode, respectively, and an Ag/AgCl as reference electrode. AP and CS-AP were dissolved in DMSO/HCl (1 mol·L^{-1}) solution, respectively. Nitrogen was pumped into the copolymer solutions for ten minutes to deoxygenate; and then CV curve was obtained with a scan rate of 20 mV·s^{-1}. Conductivity of CS-AP was measured with the four-probe method (Qianfeng Electric Co., Shanghai, China). UV–vis spectra of AP and CS-AP were measured with an UV–vis spectrophotometer (HITACHI U-3010) using the mixture of DMF and 10% (v/v) of aqueous solution of acetic acid as the solvent to determine the AP content of CS-AP.

2.3 *In vitro* cytotoxicity test

Cytotoxicity of CS and CS-AP hydrogels was evaluated using the live/dead cell staining assay and methyl thiazolyl tetrazolium (MTT) assay of PC12 cells (4×10^4 cell/plate) for 1, 2, and 3 d, respectively. And the detailed procedures were described in the section of ESI.

2.4 Animal surgery

All the experiments related to living subjects were performed in compliance with the relevant laws, ethical committee and guidelines of the Institution Animal Care and Use Committee at the Laboratory Animal Central of Sichuan University (Approval No. KS2020039). 30 Male adult Sprague Dawley (SD) rats with an age of 2 months and a weight of (200 ± 20) g were randomly divided into five groups: CS, CS-AP10, CS-AP15, CS-AP20, and autograft groups. For the autografts group, a section of sciatic nerve of 10-mm length was excised and re-implanted after inverted. For the experimental group, the sciatic nerve defect with a 10-mm length was bridged using silicone conduit and injected with different CS-AP hydrogels. Observations and operations were performed at 3 and 6 weeks, respectively. And the specific surgical procedures were described in the section of ESI. In order to avoid effect of non-degradable silicon conduit, two degradable conduits with 14-mm of length and 2-mm of internal diameter which were rolled from two parallel fiber-films of poly-L-lactic acid (PLLA) were used to further analyze the function of CS-AP, and then the proximal and distal nerve stumps were sutured in 1.0 mm inside the degradable conduit, subsequently, CS-AP10 was injected into one of PLLA conduit, named as PLLA conduit + CS-AP10.

2.5 Analysis of functional recovery

Sciatic functional index (SFI) was analyzed with the walking track to assess functional recovery of repair nerve. Briefly, rats were placed in a purpose-built runway with a dark shelter at the end after their hind feet were fully dipped in black ink. The experiment was repeated three times for each rat, and their footprints were collected. Following indexes were measured and collected, including the distance between the third toe to the heal stood for the paw length (PL), the first toe to the fifth toe stood for toe spread (TS), the second toe to the fourth toe stood for intermediary toe spread (IT), and those data were divided into the two larger groups of the normal (N) and the experimental (E) legs. SFI was calculated using the following formula [21]:

$$\mathrm{SFI} = -38.3\times\frac{\mathrm{EPL}-\mathrm{NPL}}{\mathrm{NPL}} + 109.5\times\frac{\mathrm{ETS}-\mathrm{NTS}}{\mathrm{NTS}} + 13.3\times\frac{\mathrm{EIT}-\mathrm{NIT}}{\mathrm{NIT}} - 8.8 \quad (1)$$

Zero of SFI meant totally recovery of sciatic nerves function, while −100 of SFI indicated a complete loss of nerve function.

2.6 Histological analysis

Regenerated nerves were dissected and treated through hematoxylin-eosin (HE) staining, toluidine blue (TB) staining, and histological changes were observed with fluorescence microscope, and the sample preparation procedures were shown in the section of ESI. Myelin morphology was observed using TEM (JEM-1400plus, JEOL, Japan) in order to analyze the axonal area and myelin thickness.

2.7 Immunofluorescent analysis

At 3 and 6 weeks of post-operation, the regenerated nerves were harvested from SD rats and fixed with 4% of paraformaldehyde. Then the samples were fixed by 1% of osmium tetroxide, post-dehydrated, and embedded in paraffin. All samples were evaluated by NF200, S100, and DAPI triple immunofluorescent staining. The primary antibodies were anti-NF200 and anti-S100 beta. The cross-sections of regenerated nerve images were observed under an immunofluorescence microscope. The experiment was repeated three times.

2.8 Statistical analysis

All the experimental data analysis from the studies was performed using SPSS Statistics 20. They were expressed as mean ± standard deviation. The significant differences among different samples were investigated with one-way analysis of variance (ANOVA, $p < 0.05$), and the significant differences between each experimental group and control group were analyzed by the Dunnett-*t* test, and the significant difference between two experimental groups was analyzed with the least significant difference (LSD) test.

3 Results and discussion

3.1 Composition and properties of CS-AP

Different content AP was grafted on the macromolecule chain of CS with an amination reaction between the amine group of CS and the carboxyl group of AP. FT-IR spectra of CS, AP, and CS-AP20 hydrogel were shown in Fig. S2. Compared with the spectra of CS and AP, there were the characteristic peaks at 1021 and 1660 cm^{-1} from CS in Curve c of CS-AP20, but also an absorption peak at 1498 cm^{-1} corresponding to the quinoid ring from AP, demonstrating that the AP short chains were successfully linked with CS chains [25].

UV–vis spectra of two samples were shown in Fig. 1(a), and two absorbance peaks at about 308 and 620 nm were assigned to the π–π* transition of the aromatic benzene ring and the benzenoid to quinoid excitonic transition, respectively [26]. When AP short-chains were doped with acid, there was a peak at 430 nm in the UV–vis spectra of AP and CS-AP10, respectively, due to the formation of polarons after doping acid in AP. The peaks from the benzene ring slightly shifted from 308 nm of AP to 300 nm of CS-AP10 samples, resulting from the decrease in the effective conjugation length of the AP segment in the AP-crosslinked CS and the non-planar conformation of the AP segments. The contents of AP in the products were also determined by UV–vis spectra, and the results in Table S1 showed that AP contents in three samples of CS-AP10, CS-AP15, and CS-AP20 were 4.42, 5.68, and 7.32 wt.%, respectively.

^{1}H NMR spectra of AP and CS-AP20 were shown in Fig. 1(b). In the curve of AP, there were three equal-strength and equidistant peaks at δ values of 6.94, 7.07, and 7.20, assigned to the polyaniline which were directly correlated with the protonation of the AP backbone. In the curve of CS-AP20, the proton signals at δ values of 3.48, 2.51, and 1.60 were assigned to the hydroxyl and alkyl groups of CS and similar triplet peaks were also observed [27]. These results indicated that AP was successfully linked with chitosan chains, and the structural integrality of AP remained.

XRD patterns of CS, AP, and CS-AP polymers were shown in Fig. 1(c). Two sharper peaks centered at 19.2° and 25.1° appeared at the pattern of AP, indicating its lower crystallinity. The peaks centered at 19.2° ((1 0 0) face) and 25.1° ((1 1 0) face) were ascribed to the periodicity parallel and perpendicular to the polymer chains of AP, respectively. Two stronger peaks in the diffractogram of CS at 2θ of 11.8° and 19.9°, from the crystal forms I and II, respectively [28], were ascribed to the higher crystallinity of CS. The morphology of the prepared sample was observed under SEM, and it was found from Fig. 1(d) that there were lots of nano-bulges in the surface of the CS-AP10 sample, resulting from the accumulation of AP short-segments in the hydrogel.

The electroactive materials could be converted between the oxidation state and the reducing state, and changed into electric conductor through reversible ion exchange,

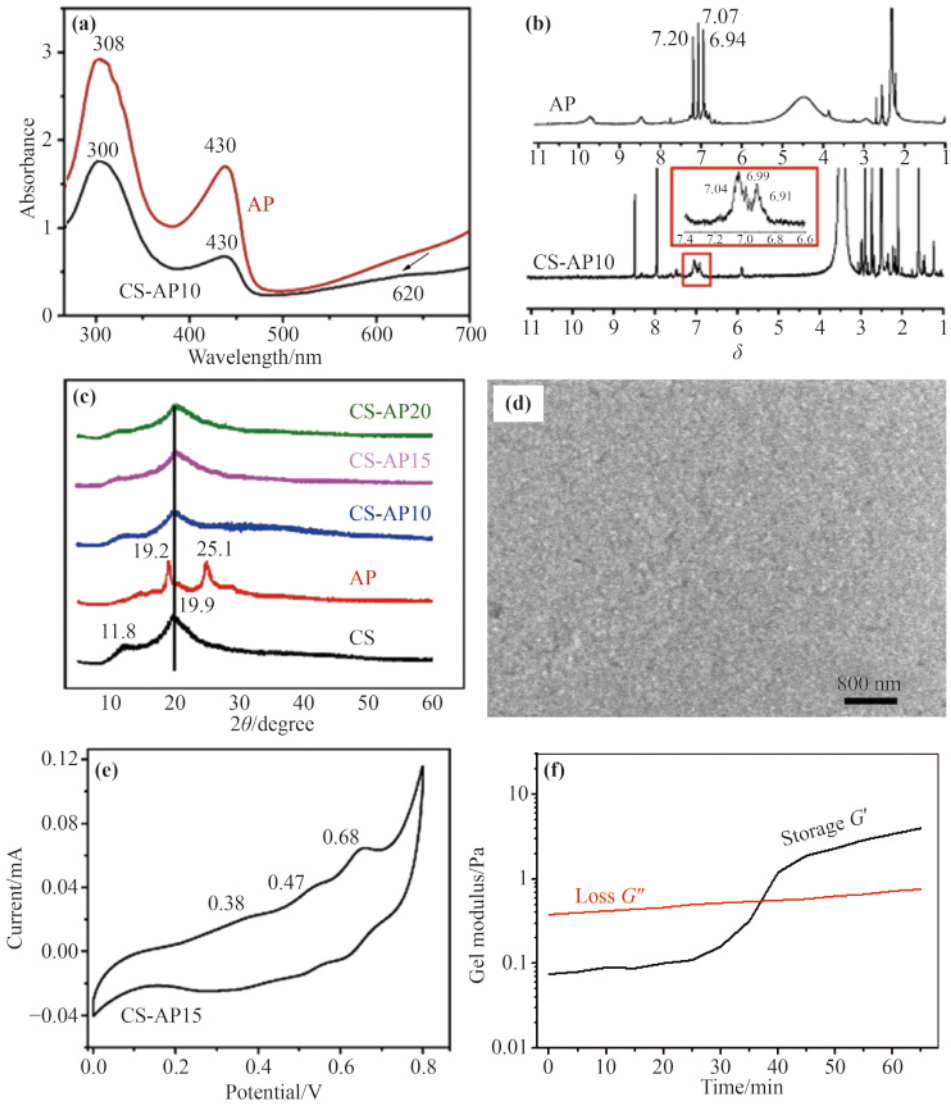

Fig. 1 Characterization results of CS-AP sample: (**a**) UV–vis spectra and (**b**) ^{1}H NMR spectra of AP and CS-AP; (**c**) XRD patterns of CS, AP and several CS-AP polymers; (**d**) SEM image, (**e**) cyclic voltammograms, and (**f**) rheological behavior of CS-AP10.

could also transmit bioelectrical signals *in vivo* and play an important role in neural activities. CV curves of CS-AP10 hydrogel were shown in Fig. 1(e). There were three pairs of reversible redox peaks in two CV curves, and the well-defined oxidation peak at 0.38 V was attributed to the redox process from the "emeraldine I" to the "emeraldine II" form, and the second pair of the redox potential at 0.68 V was due to the redox process from the "emeraldine II" to the "pernigraniline" oxidation state [29]. After immersion in PBS for 7 d, the loss weight of CS-AP10 reached 62.2 wt.%, suggesting the better degradability of CS-AP10. The conductivity of CS-AP10, CS-AP15, and CS-AP20 films under wetting state was measured by the four-probe method, and their conductive values were 2.97×10^{-4}, 3.25×10^{-4}, and 3.64×10^{-4} $S \cdot cm^{-1}$, respectively, which were closed to that of the normal tissue of human body [30]. The gelation of the prepared sample was measured at 37 °C of the body temperature. It was found from Fig. 1(f) that gelation time of the CS-AP10 sample was ~35 min, suggesting that capped carboxyl groups of AP could react well with $-NH_2$ of CS to form amide groups in the hydrogels. As shown in Fig. S4, the addition of AP significantly improved the Young's modulus (from 5.02 to 6.69 MPa), indicating that AP segment crosslinked CS and reinforced its mechanical strength.

3.2 Cyto-compatibility of CS-AP

Cyto-compatibility of CS-AP hydrogel was analyzed

using live/dead cell staining assay of rat Schwann cells (RSC96) and Pheochromocytomaderived cell line (PC12) cells, and their results were shown in Figs. 2(a), S5, and S6, respectively. From Day 1 to Day 3, dominant live cells with fluorescent green color were observed, and few dead cells with red fluorescent color were found in all of CS-AP groups (Fig. 2(a)), indicating that CS-AP hydrogel is not cytotoxic to both RSC96 and PC12 cells. In the case of the live cells of the experimental groups, the spindle-like cells are similar to that of the control group appeared (Fig. 2(a)). However, these cells possessed shorter axon and rounder cell body, indicating the lower adherent ability of neurocyte. PC12 cells adhered well on the hydrogel (Fig. S5), and there was little morphological difference between the experimental groups, and the cells arrangement was directional. However, the material of CS-AP obviously affected RSC96 cells, as shown in Fig. S6. With the increase of culture time, the number of living cells in the CS-AP20 group was significantly less than that in the other groups, and the cell shape was also more irregular, indicating that nerve cells of RSC96 were more sensitive to the hydrogels.

Effects of the CS-AP hydrogels on the cell viability were analyzed with MTT assay, and their results were shown in Figs. 2(b) and 2(c). The results of PC12 cells in Fig. 2(b) showed that the cell viability of each material

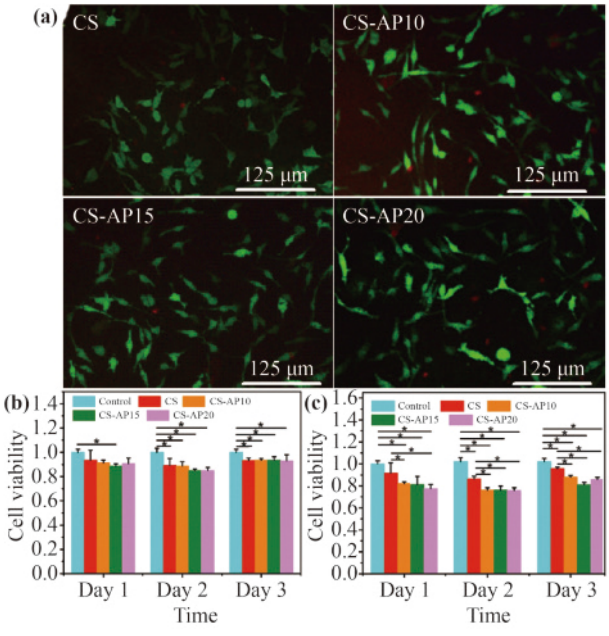

Fig. 2 (**a**) Fluorescent images of RSC96 cultured with CS and three CS-AP. Viability of (**b**) PC12 and (**c**) RSC96 cells cultured with CS and three CS-AP hydrogels for 1–3 d. All data were expressed as the mean ± SD ($n = 3$), and *$p < 0.05$.

group was higher than 80%, and there was no significant difference between each group, indicating that CS-AP hydrogel had no cytotoxicity on PC12 cells. The results of RSC96 cells in Fig. 2(c) showed that, compared with the CS group, each CS-AP hydrogel exhibited slightly lower cell activity. At the first and the second day of cell culture, the cell viability of the CS-AP10 group just reached 80%. However, with the increase of co-culture time, the cell activity at the third day was more than 80%, because RSC96 cells were sensitive to CS-AP hydrogel, exhibiting the qualified adhesion ability and cyto-compatibility of CS-AP on RSC96 cells. So for both cells of PC12 and RSC96, with the increase of the AP ratio, there was no significant difference between the experimental groups, because the electroactivity of AP segment could enhance both chemical and signal exchanges between the cells. With the increased content of AP, the effect of electroactivity on promoting cell proliferation could partly offset its toxicity [31].

3.3 Functional recovery of repair nerve

Animal experiments were carried out to analyze the repair effect of the prepared materials *in vivo*. After 3 and 6 weeks of surgery, footprints analysis was performed to evaluate the motor function recovery during sciatic nerve repair of experimental rats. As shown in Fig. S7, compared to the normal side, the length of the footprints of the experimental legs was longer while the toe spread and the intermediary toe spread was shorter, because of the loss of innervation and muscle atrophy. Compared with the footprint at 3 weeks postoperatively, the toe spread and the intermediary toe spread were significantly wider at 6 weeks postoperatively, due to the restoration of muscle function of the injured legs. SFI results at 3 and 6 weeks after surgery in Figs. S8 and 3(a) showed that the SFI values of 6 weeks were significantly higher than that of 3 weeks, suggesting partial rehabilitation of motor function. Especially, at 6 weeks after surgery, the recovery of sciatic nerves in the CS-AP10 group was significantly faster than CS-AP15 and CS-AP20 groups ($p < 0.05$), and its SFI was slightly better than that of the CS group.

3.4 Improvement of CS-AP on nerve regeneration

The surgical procedure was shown in Fig. S9. At 6 weeks after surgery, the autografted nerve was wrapped in

connective tissue, and residual un-degraded CS and CS-AP were remained in the conduit and there were no severe complications like delay of wound-healing, ulcer or infection. The images of HE-stained nerve at 3 and 6 weeks of surgery were shown in Figs. 3(c) and S10, respectively. The distribution of nerve fibers in the experimental groups at 3 weeks were scattered and disorder, compared with the autografted group, and there were many macrophages in the experimental groups, indicating an inflammatory response in the early stage of nerve repair. The proliferation or migration of Schwann cells led to their aggregation and the formation of many

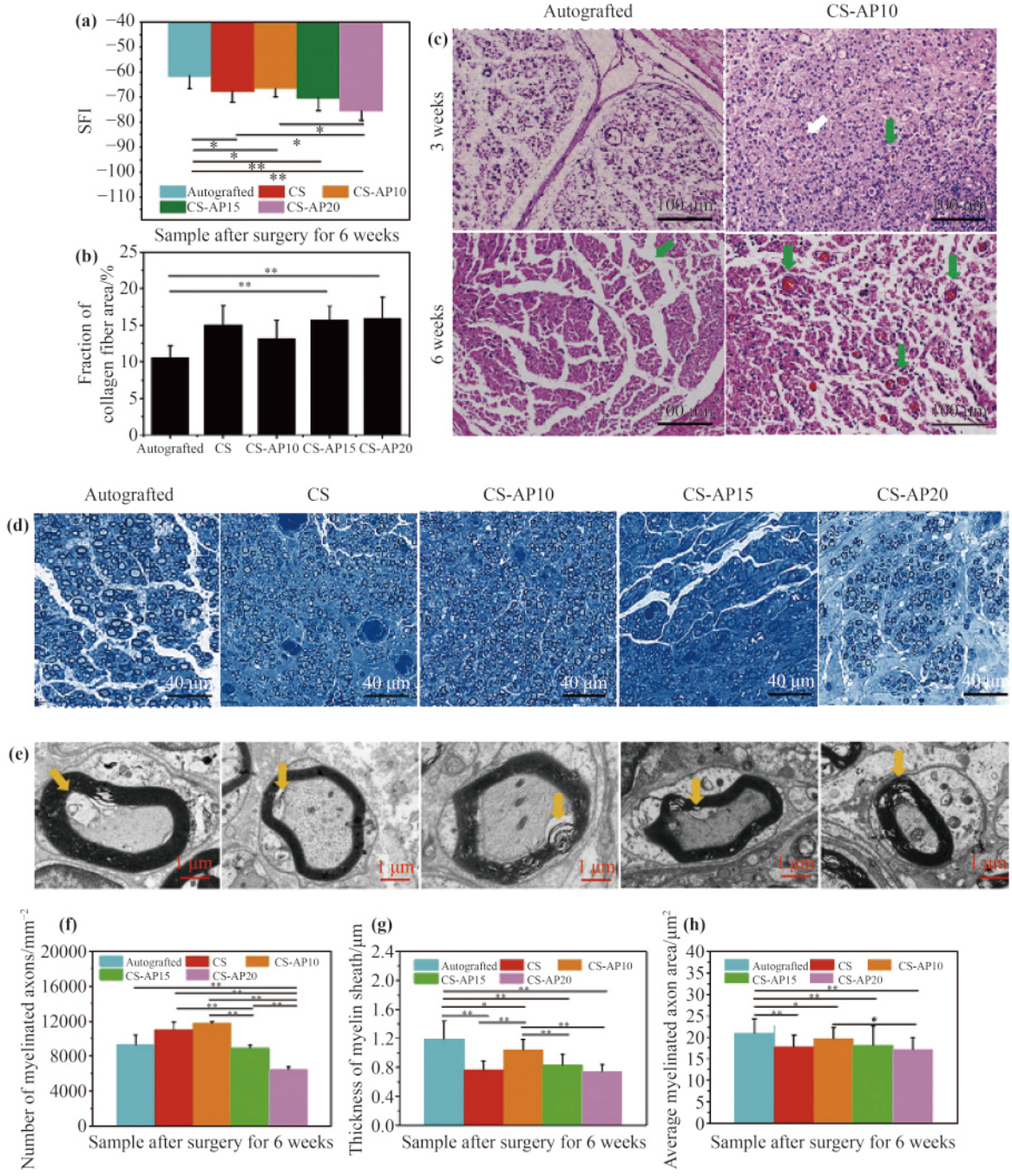

Fig. 3 (**a**) SFI values of rats at 6 weeks after surgery, and $n = 9$. (**b**) Average percentage of collagen fiber area, and $n = 15$. (**c**) Images of HE-stained nerves at 3 and 6 weeks after surgery. (**d**) Images of TB-stained nerves at 6 weeks. (**e**) TEM images of myelinated axons at 6 weeks after surgery. (**f**) The number of myelinated axons, (**g**) the thickness of myelin sheath, and (**h**) the average myelinated axon area, $n = 10$. All data were expressed as the mean ± SD, and $^{*}p < 0.05$; $^{**}p < 0.01$.

small blood vessels (indicated by green arrows in Fig. S10) in the experiment groups. There were sporadic and degrading materials with red color and irregular shape in the CS-AP10 group (indicated by white arrows in Fig. S10) in tissues, especially a large area of the residue degrading materials in CS-AP15 and CS-AP20 groups existed, due to their higher cross-linking degree. At 6 weeks of post-operation, the distribution of nerve fibers in experimental groups was still uneven. With the degradation of materials, the number of aggregated macrophages in the experimental groups was obviously decreased, indicating that the inflammatory response was reduced. Compared with 3 weeks of post-operation, there were more new blood vessels and fewer vacuoles in CS-AP groups, especially in CS-AP10 group. Images of HE-stained nerves of PLLA conduit and PLLA + CS-AP10 at 3 and 6 weeks also showed (Fig. S11) that PLLA material degrades gradually over time, and the material in PLLA conduit group at 6 weeks was degraded into fragments and wrapped by macrophages (indicated by blue arrow), indicating an inflammatory response. However, the new microvessels (indicated by red arrow) in PLLA conduit + CS-AP10 group appeared, indicating that CS-AP10 was more conducive to vascular regeneration, and the inflammatory response was lower than that in PLLA conduit group, suggesting that the electroactivity of CS-AP10 could induce differentiation & neural-factors expression of macrophages and the polarization & arrangement of Schwann cells in the repair field [32–33].

When the muscle lost the innervation, muscle fibers gradually atrophied, and the images of Masson-stained muscle were shown in Fig. S12. It is seen that the cross-sectional area of muscle fibers in CS-AP15 and CS-AP20 groups was smaller, compared with other groups. At 3 weeks, the average percentage of collagen fiber area in the autografted group was 11.84%, significantly lower than those of CS, CS-AP10, CS-AP20, and CS-AP15 groups (13.69%, 14.96%, 17.23%, and 16.13%, respectively, as shown in Fig. S13), indicating that the muscle tissue of experimental groups had not been well re-innervated in the early stage of nerve repair. Similarly, the average percentage of collagen fiber area in PLLA conduit + CS-AP10 group at 3 and 6 weeks after operation, was significantly lower than that in PLLA conduit group (Fig. S14), indicating that the muscles in PLLA conduit + CS-AP10 group were better re-innervated, and CS-AP10 material has better repair ability to nerve tissue. At 6 weeks of post-operation, there was no significant difference between any two groups, suggesting that the innervation was restored and the muscle atrophy was alleviated. As shown in Fig. 3(b), the average percentage of collagen fiber area of CS-AP10 among experiment groups was lowest, and there was no significant difference between CS-AP10 and autologous nerve group, indicating that CS-AP10 possessed a better reparability.

Images of the TB-stained nerve tissue were shown in Figs. 3(d) and S15. In images of Fig. S12, fewer myelinated axons in CS, CS-AP15, and CS-AP20 existed, and the number of myelinated axons in the CS-AP10 group was significantly higher than other experiment groups, suggesting that CS-AP10 might have the ability to induce the formation of myelin sheath by Schwann cells. The reduction and deformation of myelin sheath in the autografted group were due to the Warrer's degeneration at early stages of restoration [34]. In TEM images of 6 weeks of Fig. 3(e), the thickness of the myelinated axon of CS-AP10 group was close to that of the autografted group, higher than other groups, and the CS-AP10 group still possessed the most of myelinated axons (Fig. 3(f)). Furthermore, the average myelinated axons area of the CS-AP10 group was significantly larger than other experiment groups and only less than that of autografted groups, as shown in Fig. 3(h), demonstrating that CS-AP10 could better promote the myelin sheath regeneration, compared to the other groups.

The morphology and the thickness of the new myelin sheath were shown in Figs. 3(e), 3(g), and S16. At 6 weeks, the myelin sheaths appeared profusely in all groups, and their thicknesses were larger than those at 3 weeks. The myelin sheaths became more tightly and their structure was more orderly, due to the formation of perineurium which confined Schwann cells spatially in the process of wrapping [35]. There were some vacuoles (yellow arrow in Fig. 3(e)) in axons and defects in myelin sheaths caused by the inflammatory immune response. When the nerve injury caused a loss of nerve, a newly formed blood vessel (Fig. 3(c)) could provide not only nutrients and oxygen but also a bridge in the hydrogel of conduit for Schwann cells to migrate. AP electroactivity in hydrogel could also promote the signals communication between electrophysiologic-active cells, accelerating the nerve regeneration [36]. With the content increase of AP, CS-AP15 and CS-AP20 hydrogels were weakly cytotoxic, leading to their slower regeneration.

3.5 Discussion

Based on our above results, the primary promotion mechanism of CS-AP hydrogel on the nerve regeneration was proposed, as shown in Fig. 4. After nerve injury happened, muscles atrophied due to loss of target innervation (Fig. 4(b)), and CS-AP was injected into a conduit at the site of sciatic nerve defect (Fig. 4(a)). The insufficient neuronal regeneration was rather caused by an unfavorable growth microenvironment within the damaged nerve tissue [37], so regeneration of the damaged nerve could occur under the appropriate biological and physical stimuli. The unique electroactivity of hydrogel could upregulate the neural expression through increasing ions and molecules in the microenvironment of cell growth, and improving protein synthesis and adsorption [38]. In the early stage after implantation (Fig. 4(c)), the injected hydrogel played a role as a bridge in the directed growth of nerves with its electroactivity. The permeability and flexibility of the hydrogels promoted cell attachment and migration of neurites and vascularization, and the angiogenic process was induced by reinforcing the intracellular expression of Reca-1 and laminin due to AP electroactivity which promoted the communication of signals between cells [39]. Regenerated micrangium also guided the proliferation and migration of Schwann cells [40], and the new capillaries provided nutrition and oxygen for neuronal regeneration, relieving local hypoxia at nerve repair sites [41]. At 6 weeks of post-operation, the re-innervation restored muscle function (Fig. 4(d)). The inflammatory response was reduced with the removal of AP by macrophages (Fig. S17) and the degradation of CS and anti-inflammatory of amino groups in CS [42–43]. Finally, the remained CS-AP chains and AP during the regeneration allowed a better electrical signal delivery in the repair site to promote the re-innervation on muscles [44], leading to the functional recovery of the regeneration tissue (Figs. 4(e) and S18).

4 Conclusions

An electroactivity hydrogel was fabricated by CS crosslinked with AP, and its mechanical strength was 5.02–6.69 MPa. AP-crosslinked CS hydrogels possessed electroactivity due to reversible redox peaks at 0.38 and 0.65 V in their CV curves, and their conductivity was ~3.25×10^{-4} S·cm^{-1}. These hydrogels were almost non-cytotoxic on PC12 and RSC96 cells. The results of the repair of the sciatic nerve demonstrated that CS-AP hydrogels could significantly induce the micrangium formation and the nerve regeneration through AP

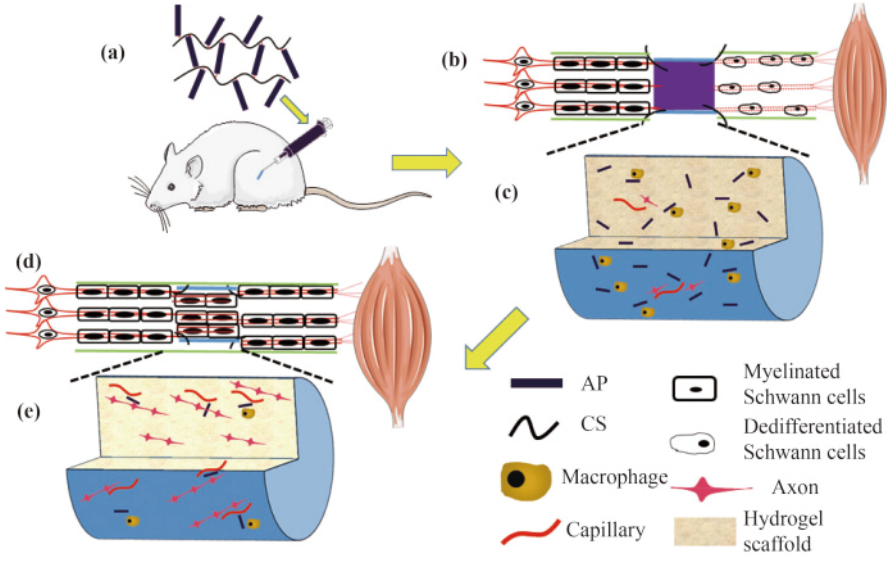

Fig. 4 (**a**) CS-AP hydrogels were injected into a conduit at the site of sciatic nerve injury; (**b**) muscles atrophied after loss of target innervation; (**c**) after the implantation, AP content in the hydrogel could guiding the remodeling of the neural regeneration microenvironment as well as promoting gene expression and adsorbing protein, allowing capillaries formation, regenerated neuronal axon growth and Schwann cell migration; (**d**) in 6 weeks of the regeneration, the re-innervation restored muscle function and muscle fibers became long and thick; (**e**) AP was cleared by macrophages and CS matrix degraded, and there was a lot of angiogenesis and regeneration of nerve tissue.

electroactivity and CS degradation, promoting the functional recovery at 6 weeks of post-operation. A mechanism for the promotion of AP-crosslinked CS hydrogels on capillary regeneration, nerve repair and muscle function restoration was proposed. These results in this study indicated the great potential of AP-crosslinked CS on the regeneration and functional recovery of peripheral nerve injury.

Acknowledgements This work was supported by National Key Research and Development Program of China (Grant No. 2018YFC1106800) and Sichuan Science and Technology Project (Grant No. 2018JY0535).

Electronic supplementary information Supplementary materials can be found in the online version at https://doi.org/10.1007/s11706-022-0614-8, which are associated with this work including Table S1 and Figs. S1–S18.

References

[1] Siemionow M, Brzezicki G. Chapter 8: Current techniques and concepts in peripheral nerve repair. International Review of Neurobiology, 2009, 87: 141–172

[2] Zhu H, Shen L, Yang M, et al. Progress in facial reinnervation. Journal of Neurorestoratology, 2021, 9(3): 177–185

[3] Schmidt C E, Leach J B. Neural tissue engineering: strategies for repair and regeneration. Annual Review of Biomedical Engineering, 2003, 5(1): 293–347

[4] Wang Y, Zhang Y, Li X, et al. The progress of biomaterials in peripheral nerve repair and regeneration. Journal of Neurorestoratology, 2020, 8(4): 252–269

[5] Javed R, Ao Q. Nanoparticles in peripheral nerve regeneration: a mini review. Journal of Neurorestoratology, 2022, 10(1): 1–12

[6] Guo B, Ma P X. Conducting polymers for tissue engineering. Biomacromolecules, 2018, 19(6): 1764–1782

[7] Ravichandran R, Sundarrajan S, Venugopal J R, et al. Applications of conducting polymers and their issues in biomedical engineering. Journal of the Royal Society Interface, 2010, 7(Suppl 5): S559–S579

[8] Bendrea A D, Cianga L, Cianga I. Review paper: progress in the field of conducting polymers for tissue engineering applications. Journal of Biomaterials Applications, 2011, 26(1): 3–84

[9] Wu Q, Pan C, Hu Y, et al. Neuroprotective effects of adipose-derived stem cells on ferrous sulfate-induced neurotoxicity. Brain Science Advances, 2021, 7(3): 172–183

[10] Zarrintaj P, Zangene E, Manouchehri S, et al. Conductive biomaterials as nerve conduits: recent advances and future challenges. Applied Materials Today, 2020, 20: 100784

[11] Zare E N, Makvandi P, Ashtari B, et al. Progress in conductive polyaniline-based nanocomposites for biomedical applications: a review. Journal of Medicinal Chemistry, 2020, 63(1): 1–22

[12] Liu J, Kim Y S, Richardson C E, et al. Genetically targeted chemical assembly of functional materials in living cells, tissues, and animals. Science, 2020, 367(6484): 1372–1376

[13] Ma X, Ge J, Li Y, et al. Nanofibrous electroactive scaffolds from a chitosan-grafted-aniline tetramer by electrospinning for tissue engineering. RSC Advances, 2014, 4(26): 13652–13661

[14] Guo B L, Finne-Wistrand A, Albertsson A C. Simple route to size-tunable degradable and electroactive nanoparticles from the self-assembly of conducting coil–rod–coil triblock copolymers. Chemistry of Materials, 2011, 23(17): 4045–4055

[15] Zarrintaj P, Bakhshandeh B, Saeb M R F, et al. Oligoaniline-based conductive biomaterials for tissue engineering. Acta Biomaterialia, 2018, 72: 16–34

[16] Dong R, Zhao X, Guo B, et al. Biocompatible elastic conductive films significantly enhanced myogenic differentiation of myoblast for skeletal muscle regeneration. Biomacromolecules, 2017, 18(9): 2808–2819

[17] Chen J, Yu M, Guo B, et al. Conductive nanofibrous composite scaffolds based on *in-situ* formed polyaniline nanoparticle and polylactide for bone regeneration. Journal of Colloid and Interface Science, 2018, 514: 517–527

[18] Guo B L, Finne-Wistrand A, Albertsson A C. Enhanced electrical conductivity by macromolecular architecture: hyperbranched electroactive and degradable block copolymers based on poly(ε-caprolactone) and aniline pentamer. Macromolecules, 2010, 43(10): 4472–4480

[19] Zhang L, Wang L, Guo B, et al. Cytocompatible injectable carboxymethyl chitosan/N-isopropylacrylamide hydrogels for localized drug delivery. Carbohydrate Polymers, 2014, 103: 110–118

[20] Li P, Poon Y F, Li W, et al. A polycationic antimicrobial and biocompatible hydrogel with microbe membrane suctioning ability. Nature Materials, 2011, 10(2): 149–156

[21] Bain J R, Mackinnon S E, Hunter D A. Functional evaluation of complete sciatic, peroneal, and posterior tibial nerve lesions in the rat. Plastic and Reconstructive Surgery, 1989, 83(1): 129–136

[22] Guan H, Xie Z, Zhang P, et al. Synthesis and characterization of biodegradable amphiphilic triblock copolymers containing L-glutamic acid units. Biomacromolecules, 2005, 6(4): 1954–1960

[23] Feng Y Y, Bai S, Li G G, et al. Reprogramming rat astrocytes into neurons using small molecules for cell replacement following intracerebral hemorrhage. Brain Science Advances, 2021, 7(3): 184–198

[24] de Medinaceli L, Freed W J, Wyatt R J. An index of the functional condition of rat sciatic nerve based on measurements made from walking tracks. Experimental Neurology, 1982,

77(3): 634–643

[25] Zong Z, Kimura Y, Takahashi M, et al. Characterization of chemical and solid state structures of acylated chitosans. Polymer, 2000, 41(3): 899–906

[26] Hu J, Huang L, Zhuang X, et al. Electroactive aniline pentamer cross-linking chitosan for stimulation growth of electrically sensitive cells. Biomacromolecules, 2008, 9(10): 2637–2644

[27] Wang X, Sun T, Wang C, et al. ^{1}H NMR determination of the doping level of doped polyaniline. Macromolecular Chemistry and Physics, 2010, 211(16): 1814–1819

[28] Liu Y, Hu J, Zhuang X, et al. Synthesis and characterization of novel biodegradable and electroactive hydrogel based on aniline oligomer and gelatin. Macromolecular Bioscience, 2012, 12(2): 241–250

[29] Chao D, Ma X, Lu X, et al. Design, synthesis and characterization of novel electroactive polyamide with amine-capped aniline pentamer in the main chain via oxidative coupling polymerization. Journal of Applied Polymer Science, 2007, 104(3): 1603–1608

[30] Qazi T H, Rai R, Dippold D, et al. Development and characterization of novel electrically conductive PANI–PGS composites for cardiac tissue engineering applications. Acta Biomaterialia, 2014, 10(6): 2434–2445

[31] Bagheri B, Zarrintaj P, Samadi A, et al. Tissue engineering with electrospun electro-responsive chitosan-aniline oligomer/ polyvinyl alcohol. International Journal of Biological Macromolecules, 2020, 147: 160–169

[32] Bagher Z, Atoufi Z, Alizadeh R, et al. Conductive hydrogel based on chitosan-aniline pentamer/gelatin/agarose significantly promoted motor neuron-like cells differentiation of human olfactory ecto-mesenchymal stem cells. Materials Science and Engineering C, 2019, 101: 243–253

[33] Liu S, Wang J, Zhang D, et al. Investigation on cell biocompatible behaviors of polyaniline film fabricated via electroless surface polymerization. Applied Surface Science, 2010, 256(11): 3427–3431

[34] Stoll G, Jander S, Myers R R. Degeneration and regeneration of the peripheral nervous system: from Augustus Waller's observations to neuroinflammation. Journal of the Peripheral Nervous System, 2002, 7(1): 13–27

[35] Tang X, Xue C, Wang Y, et al. Bridging peripheral nerve defects with a tissue engineered nerve graft composed of an *in vitro* cultured nerve equivalent and a silk fibroin-based scaffold. Biomaterials, 2012, 33(15): 3860–3867

[36] Kaur G, Adhikari R, Cass P, et al. Electrically conductive polymers and composites for biomedical applications. RSC Advances, 2015, 5(47): 37553–37567

[37] Richardson P M, McGuinness U M, Aguayo A J. Axons from CNS neurons regenerate into PNS grafts. Nature, 1980, 284(5753): 264–265

[38] Schmidt C E, Shastri V R, Vacanti J P, et al. Stimulation of neurite outgrowth using an electrically conducting polymer. Proceedings of the National Academy of Sciences of the United States of America, 1997, 94(17): 8948–8953

[39] Domínguez-Bajo A, González-Mayorga A, Guerrero C R, et al. Myelinated axons and functional blood vessels populate mechanically compliant rGO foams in chronic cervical hemisected rats. Biomaterials, 2019, 192: 461–474

[40] Carmeliet P, Tessier-Lavigne M. Common mechanisms of nerve and blood vessel wiring. Nature, 2005, 436(7048): 193–200

[41] Xia B, Lv Y. Dual-delivery of VEGF and NGF by emulsion electrospun nanofibrous scaffold for peripheral nerve regeneration. Materials Science and Engineering C, 2018, 82: 253–264

[42] Zhang X, Qi H, Wang S, et al. Cellular responses of aniline oligomers: a preliminary study. Toxicology Research, 2012, 1(3): 201–205

[43] Zhao Y, Wang Y, Gong J, et al. Chitosan degradation products facilitate peripheral nerve regeneration by improving macrophage-constructed microenvironments. Biomaterials, 2017, 134: 64–77

[44] Chen X, Liu C, Huang Z, et al. Preparation of carboxylic graphene oxide-composited polypyrrole conduits and their effect on sciatic nerve repair under electrical stimulation. Journal of Biomedical Materials Research Part A, 2019, 107(12): 2784–2795